



## Theoretical studies of strong-field photoionization of CH<sub>3</sub>I

Fan Shi<sup>a,b</sup>, Yingfeng Zhang<sup>a,b</sup>, Ji Qi<sup>a,b</sup>, Hongwei Song<sup>a,\*</sup>, Minghui Yang<sup>a,\*</sup>

<sup>a</sup> State Key Laboratory of Magnetic Resonance and Atomic and Molecular Physics, Wuhan Institute of Physics and Mathematics, Chinese Academy of Sciences, Wuhan 430071, China

<sup>b</sup> University of Chinese Academy of Sciences, Beijing 100049, China

### ABSTRACT

The CH<sub>3</sub>I molecule serves as an important model system in photochemistry. The photoionization usually includes the laser-molecule interaction and ionization process. Theoretical simulations of the laser-induced ionization process are, however, difficult due to multi-electrons involved. In this work, the ionization process of CH<sub>3</sub>I is studied based on the Frank-Condon principle. Three two-dimensional potential energy surfaces along the C–I bond length and the H–C–I umbrella angle are constructed for the ground electronic state of CH<sub>3</sub>I and the ground and first excited states of CH<sub>3</sub>I<sup>+</sup>, with internally contracted multireference configuration interaction method and the aug-cc-pVTZ basis set used for the atoms C and H and the aug-cc-pvtz-pp basis set for the atom I. The vibrational frequencies of the C–I stretching mode and the umbrella mode of CH<sub>3</sub> are calculated for both CH<sub>3</sub>I and CH<sub>3</sub>I<sup>+</sup>, and are consistent with the experimental measurements. Furthermore, based on the Ammosov-Delone-Krainov ionization model, dynamics calculations are carried out to simulate ionization process induced by *R*-selective depletion mechanism and the vibrational wave packet motion on CH<sub>3</sub>I<sup>+</sup> PESs.

### 1. Introduction

Methyl iodide is a prototypical system for understanding polyatomic molecular photodissociation dynamics. Much work has been done on the spectroscopy and photochemistry of CH<sub>3</sub>I due to its importance in industry and environment [1–8]. Aside from the extensive studies on the photodissociation dynamics of CH<sub>3</sub>I and its isotopomers, the photoionization dynamics of CH<sub>3</sub>I and the subsequent photodissociation of CH<sub>3</sub>I<sup>+</sup> has also attracted particular attention since the first high resolution photodissociation spectrum was reported by McGilvery and Morrison [9]. The CH<sub>3</sub>I<sup>+</sup> exhibits a strong absorption in the visible band of the spectrum corresponding to the formation of CH<sub>3</sub><sup>+</sup>, thus making it a good candidate for studying ion photodissociation. On the other hand, spin-orbit interaction, vibronic interaction and Coriolis effect are expected to affect its rotational structure [10]. Besides, methyl iodide and its cation have been proven to be an excellent system for the demonstration of new experimental techniques [11–19].

The photodissociation mechanism of CH<sub>3</sub>I<sup>+</sup> is still unclear although many experimental studies focus on the photodissociation of low-lying excited states jumping from the ground electronic state [16–18]. Goss et al. [13,14] determined the vibrational frequencies of CH<sub>3</sub>I<sup>+</sup> by analyzing the photodissociation spectra for the A<sup>2</sup>A<sub>1</sub> → X<sup>2</sup>E<sub>3/2</sub> transition. Chupka and his co-workers [20] measured the photodissociation spectra and determined the dissociation threshold for the methyl cation and the iodine cation. The dissociation pathways and the associated dissociated fragments of CH<sub>3</sub>I<sup>+</sup> were examined by Loch et al. [21]

using two distinct setups experimentally [22,23] and DFT calculations theoretically. Merkt and his co-workers [24,25] reported a high-resolution photoelectron spectroscopic study of the combined Jahn–Teller and spin–orbit interactions in the methyl iodide cation using a vacuum ultraviolet (VUV) laser source with a bandwidth of 0.008 cm<sup>−1</sup>. Very recently, Poullain et al. [26] performed a combined experimental and theoretical study of the photodissociation of CH<sub>3</sub>I<sup>+</sup>. A velocity map imaging (VMI) technique incorporated with nanosecond laser pulses was employed to explore the one-color and two-color photodissociation dynamics of CH<sub>3</sub>I<sup>+</sup>. The measured translational energy distributions for the CH<sub>3</sub><sup>+</sup> and I<sup>+</sup> ions indicate two different dissociation processes. Meanwhile, theoretical calculations were carried out using multi-reference method considering single and double excitations from CASSCF wavefunctions (MRCISD). The relativistic correction and spin-orbit (SO) coupling were also taken into account in their calculations. The Boltzmann-type unstructured distribution at low energies as well as a recoiled narrow structure at higher energies observed in the experiment were all explained by the direct and indirect dissociation on a repulsive state from manifold of state.

Very recently, Loh's and our groups [27] cooperatively studied vibrational wave packet generation mechanism in neutral CH<sub>3</sub>I and multimode coherent vibrational motion in cationic CH<sub>3</sub>I<sup>+</sup>. Thanks to the exquisite sensitivity of femtosecond extreme ultraviolet absorption spectroscopy to sub-picometer structural changes, both *R*-selective depletion and bond softening-induced vibrational wave packets were observed. As signatures of coherent vibrational motion in the time-

\* Corresponding authors.

E-mail addresses: [hwsong@wipm.ac.cn](mailto:hwsong@wipm.ac.cn) (H. Song), [yangmh@wipm.ac.cn](mailto:yangmh@wipm.ac.cn) (M. Yang).

dependent spectra provide vibronic coupling strengths involving core-level transitions, the geometrical parameters of transient core-excited states were determined.

This work reported the theoretical studies of  $\text{CH}_3\text{I}^+$  and  $\text{CH}_3\text{I}$  with multi-reference configuration interaction. Three two-dimensional potential energy surfaces (PESs) describing the ground electronic state of  $\text{CH}_3\text{I}$  and the ground and first excited electronic states of  $\text{CH}_3\text{I}^+$  along the C–I stretching and H–C–I umbrella modes will be constructed using the neural network method, in which the *ab initio* energies are calculated at the level of MRCI + Q. Dynamics calculations will be performed to simulate the vibrational wave packet motion induced by the R-selective depletion mechanism. The remainder of the paper is organized as follows. Section 2 outlines briefly the methodology. The results and discussion are presented in Section 3, followed by conclusions in Section 4.

## 2. Theory

### 2.1. Potential energy surface

The *ab initio* calculations are carried out with state-averaged complete active space self-consistent field (SA-CASSCF) and internally contracted multireference configuration interaction method with the Davidson correction (MRCI + Q) [28,29] and the augmented correlation-consistent polarized valence triple zeta basis set (aug-cc-pVTZ) is employed for the atoms C and H and the relativistic effective core potentials (RECP) basis aug-cc-pvtz-pp for the atom I, using the MOLPRO 2010.1 program package [3,28,31]. The active space considered in this study contains five electrons and four molecular orbitals:  $\sigma$ -bonding,  $\sigma$ -antibonding and  $5p_x/5p_y$  orbitals of iodine atom. Six electronic states are included in SA-CASSCF calculations with equal weight for both neutral  $\text{CH}_3\text{I}$  and cationic  $\text{CH}_3\text{I}^+$ . Test calculations show that including six electronic states could produce smooth potential energy curves. In addition, the spin-orbit eigenstates are obtained by diagonalizing the full Breit-Pauli Hamiltonian  $\hat{H}^{\text{el}} + \hat{H}^{\text{SO}}$  in the basis of eigenfunctions of  $\hat{H}^{\text{el}}$ .

To construct the two-dimensional (2D) potential energy surface, the *ab initio* points are sampled by a two-dimensional grid. The H–C–I angle is taken from  $60^\circ$  to  $135^\circ$  with an interval of  $5^\circ$  and the bond length C–I is selected from 1.6 to  $25.0 \text{ \AA}$  with an uneven internal, yielding 4226 points. After truncating the energy to 5.7 eV for the ground state and 3.0 eV for the first-excited state with respect to the global minimum of  $\text{CH}_3\text{I}^+$ , a total of 3601 points and 1925 points are retained to construct the PES of the ground state and the first-excited state, respectively. The three 2D PESs are fitted independently. The robust neural-network (NN) method is employed in the fitting [32]. In each NN fitting, the dataset is divided randomly into two sets, namely the training (95%) and validation (5%) sets. The training data is then fitted by backward propagation neural network with the Levenberg-Marquardt algorithm. The structure of the neural network is 2-20-20-1, which contains 2 internal coordinates as input, 20 and 20 neurons in two hidden layers, and 1 output of potential energy. The inputs in the NN fitting are taken as the bond length C–I  $R$  and the H–C–I angle  $\theta$ . The root mean squared errors of the three PESs are 2.86, 2.74 and 2.68 meV for the ground state of  $\text{CH}_3\text{I}$ , the ground and first excited states of  $\text{CH}_3\text{I}^+$ .

### 2.2. Quantum dynamics

In the two-dimensional model, the  $\text{CH}_3$  moiety in  $\text{CH}_3\text{I}^+$  is assumed to keep  $C_{3v}$  symmetry. The coordinates  $R$  is the bond length of C–I is denoted as and the angle of H–C–I is denoted as  $\theta$ . The two-dimensional ADK Hamiltonian in the coordinates  $(R, \theta)$  is expressed as:

$$\hat{H} = -\frac{1}{2\mu_R} \frac{\partial^2}{\partial R^2} + \frac{\sin \theta \cos \theta}{\rho^2} \left( \frac{1}{\mu_x} - \frac{1}{\mu_s} \right) \frac{\partial}{\partial \theta} - \frac{1}{2\rho^2} \left( \frac{\cos^2 \theta}{\mu_x} + \frac{\sin^2 \theta}{\mu_s} \right) \frac{\partial^2}{\partial \theta^2} + \hat{V}(R, \theta), \quad (1)$$

where  $\mu_R$  is the reduced mass of  $\text{CH}_3\text{I}^+$ .  $\mu_x$  and  $\mu_s$  are the reduced masses of  $\text{H}_3$  and  $\text{CH}_3$ , respectively.  $\rho$  is the bond length of C–H, which is fixed at  $1.082 \text{ \AA}$ , corresponding to the equilibrium geometry of  $\text{CH}_3\text{I}^+$ . The vibrational energies of  $\text{CH}_3\text{I}$  and  $\text{CH}_3\text{I}^+$  on the ground and/or first excited electronic states are obtained by diagonalizing the 2D Hamiltonian on their individual PESs.

The time-dependent wave function is expanded as

$$\psi(R, \theta; t) = \sum_{n_R, m_\theta} a_{n_R, m_\theta}(t) Q_{n_R}(R) Q_{m_\theta}(\theta), \quad (2)$$

where  $a_{n_R, m_\theta}(t)$  are time-dependent coefficients.  $n_R$  and  $m_\theta$  are the labels for basis functions of  $R$  and  $\theta$ , respectively.  $Q_{n_R}(R)$  and  $Q_{m_\theta}(\theta)$  are sine basis functions.

The wave function is propagated using the split-operator method,

$$\psi(t + \Delta) = e^{-i\hat{T}\Delta/2} e^{-i\hat{V}\Delta} e^{-i\hat{T}\Delta/2} \psi(t), \quad (3)$$

in which the total Hamiltonian is split into two terms as  $\hat{H} = \hat{T} + \hat{V}$ .

The time-evolution of the C–I bond distance  $R$  and the umbrella angle  $\theta$  is defined as

$$\begin{aligned} \langle R(t) \rangle &= \langle \psi(R, \theta; t) | R | \psi(R, \theta; t) \rangle \\ \langle \theta(t) \rangle &= \langle \psi(R, \theta; t) | \theta | \psi(R, \theta; t) \rangle \end{aligned} \quad (4)$$

Since the R-selective depletion mechanism is simulated in this work, the Ammosov–Delone–Krainov (ADK) ionization rates [33] are employed to deplete the wave functions of the neutral  $\text{CH}_3\text{I}$ . It should be a good approximation considering that ionization involving the lone-pair electrons of iodine with predominantly atomic  $5p$  character. The ionization rate is given by

$$\begin{aligned} W(R, \theta, r; t) &= 41.34 C_{n^*}^2 I_f(l, m) E(R, \theta) \left( \frac{3F(r, t)}{\pi(2E(R, \theta))^{3/2}} \right)^{1/2} \left( \frac{2}{F(r, t)} (2E(R, \theta))^{3/2} \right)^{2n^* - |m| - 1} \\ &\quad \times \exp\left( -\frac{2}{3F(r, t)} (2E(R, \theta))^{3/2} \right), \end{aligned} \quad (5)$$

where the factor  $C$  and  $F$  are given by

$$C_{n^*l} = \left( \frac{2e}{n^*} \right)^{n^*} \frac{1}{(2\pi n^*)^{1/2}} \quad (6)$$

and

$$f(l, m) = \frac{(2l+1)(1+|m|)}{2^{|m|} (|m|)! (1-|m|)!}, \quad (7)$$

in which  $e = 2.71828$ ,  $m = 0$  and  $l = 0$ .  $F(r, t)$  is the electronic of the laser and expressed as

$$F(r, t) = 0.0696271 * 2^{-t/18} \exp\left( -\frac{r^2}{10000} \right) |\cos(2.51154 t)|. \quad (8)$$

$E(R, \theta)$  is the ionization potential and defined as

$$E(R, \theta) = V^{\text{CH}_3\text{I}^+}(R, \theta) - V^{\text{CH}_3\text{I}}(R, \theta), \quad (9)$$

in which  $V^{\text{CH}_3\text{I}^+}(R, \theta)$  and  $V^{\text{CH}_3\text{I}}(R, \theta)$  are the potential energies of the ground electronic states of the cationic  $\text{CH}_3\text{I}^+$  and the neutral  $\text{CH}_3\text{I}$ , respectively. Then, the effective principle quantum number can be obtained by

$$n^* = Z / \sqrt{2E(R, \theta)}, \quad (10)$$

where  $Z$  is the charge of  $\text{CH}_3\text{I}^+$  and taken as + 1.

The initial wave packet is constructed as the product of the eigenfunction of the neutral  $\text{CH}_3\text{I}$  and the square root of the ionization fraction:

**Table 1**  
Equilibrium geometries of the ground and first excited electronic state of  $\text{CH}_3\text{I}^+$ .

		$R_{\text{C-I}}/\text{\AA}$	$R_{\text{C-H}}/\text{\AA}$	$\text{A}_{\text{H-C-I}}/\text{degrees}$
$\text{CH}_3\text{I}^+(\text{X}^2\text{E}_{3/2})$	DFT/B3LYP/aug-cc-Pvtz [34]	2.169	1.082	107.7
	MP2 [26]	2.133	1.077	107.6
	Exp. [34]	$2.126 \pm 0.002$	$1.091 \pm 0.002$	$108.3 \pm 0.3$
	MRCI <sup>a</sup>	2.170	1.082	107.7
	UCCSD(T) <sup>a</sup>	2.154	1.088	107.2
$\text{CH}_3\text{I}^+(\text{A}^2\text{A}_1)$	SODFT/B3LYP/aug-cc-pVTZ [34] SODFT	2.180	1.086	105.6
	Exp. [34]	$2.503 \pm 0.015$	$1.072 \pm 0.009$	$98.2 \pm 3.7$
	MRCI <sup>a</sup>	2.162	–	105.2

<sup>a</sup> This work, the basis set is C,H = avtz; I = avtz-pp.

$$\psi(R, \theta; t = 0) = \sqrt{f(R, \theta)} \varphi_i(R, \theta), \quad (11)$$

where  $i$  denotes the  $i$ th eigenstate of  $\text{CH}_3\text{I}$ . The ionization fraction  $f$  is calculated by

$$f(R, \theta) = \frac{\iint W(R, r, \theta, t) A_{XUV}(r) 2\pi r dr dt}{\iint A_{XUV}(r) 2\pi r dr dt}, \quad (12)$$

in which  $A_{XUV}(r)$  is the Gaussian beam and expressed as

$$A_{XUV}(r) = \exp\left(-\frac{2r^2}{100^2}\right). \quad (13)$$

In the calculation, 80 sine discrete variable representation (DVR) basis/grids are used for the C–H bond coordinate  $R$  in a range from 3.5 to 5.5  $a_0$  and 240 sine DVR basis/grids for the H–C–I umbrella angle  $\theta$  ranging from 50° to 140°.

### 3. Results and discussion

The equilibrium geometry of  $\text{CH}_3\text{I}^+$  in the ground electronic state is optimized by both MRCI and UCCSD(T) methods. Table 1 shows the calculated equilibrium geometry, together with some available experimental and theoretical results for comparison. It can be seen that the UCCSD(T) results agree well with the MRCI values, with the bond-distance difference less than 0.02 Å and the angle difference less than 0.5°. And these values are all in good accord with the corresponding experimental measurements [34]. Interestingly, the DFT calculations performed by Bae et al. [34] give nearly the same values as the MRCI calculations. The MP2 method [26], by happy coincidence, predicts the closest C–I bond distance to the experimental value. The equilibrium geometry of  $\text{CH}_3\text{I}^+$  in the first excited electronic state is also optimized by the MRCI method. Again, the MRCI values are in good agreement with the SODFT results [34]. They are both close to the experimental measurements, although the conformity is not as good as for the ground state.

The one-dimensional potential energy curves of several low-lying electronic states of  $\text{CH}_3\text{I}^+$  along the C–I bond length are shown in Fig. 1 with the other coordinates relaxed. The vertical ionization energy of  $\text{CH}_3\text{I}$  from the ground state of  $\text{CH}_3\text{I}$  is determined to be 9.50 eV to the ground electronic state of  $\text{CH}_3\text{I}^+$  and 12.33 eV to the first excited electronic state of  $\text{CH}_3\text{I}^+$ . These values are compared with other available experimental and theoretical results in Table 2. The agreement is good for the ground electronic state of  $\text{CH}_3\text{I}^+$  and becomes a little bit worse but acceptable for the first excited electronic state. Table 2 also displays the dissociation energies of  $\text{CH}_3\text{I}^+$  to the dissociation channels  $\text{CH}_3^+ + \text{I}^+(\text{P}_{3/2})$  and  $\text{CH}_3 + \text{I}^+(\text{P}_2)$ , which are in accord with the experimental values [35].

The C–I stretching and umbrella modes are the two most important motions of  $\text{CH}_3\text{I}$  and  $\text{CH}_3\text{I}^+$ . Here three two-dimensional PESs are constructed to for the ground electronic state of neutral  $\text{CH}_3\text{I}$  and the ground and first excited electronic states of  $\text{CH}_3\text{I}^+$ . The aforementioned

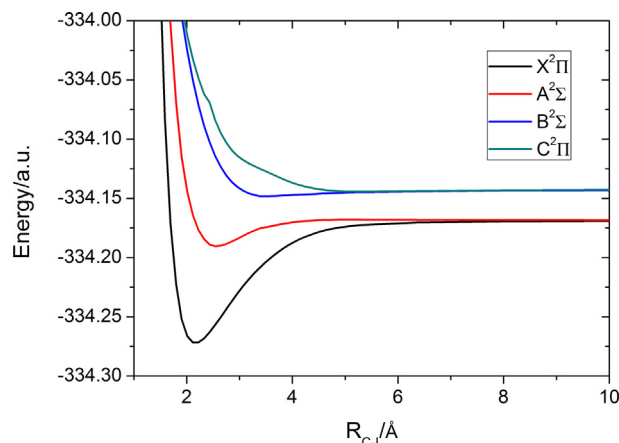


**Fig. 1.** Potential energy curves of several low-lying states of  $\text{CH}_3\text{I}^+$  along the dissociation coordinate of C–I.

two-dimensional Hamiltonian is then used to solve the bound state of with the three PESs. Table 3 shows the calculated frequencies. The theoretical frequencies are in reasonable agreement with the experimental values, with the largest difference being 99  $\text{cm}^{-1}$  for the umbrella mode in the ground state of  $\text{CH}_3\text{I}^+$ . It appears that the new PESs describe better the C–I stretching motion than the umbrella motion.

To simulate the vibrational wave packet launched by  $R$ -selective depletion, the ADK model is employed to calculate the ionization rate. At the experimental temperature of 353 K, the neutral  $\text{CH}_3\text{I}$  mainly populates in its first four eigenstates, the ground state, the fundamental and first overtone of the C–H stretching mode, the fundamental of the umbrella mode, with respective Boltzmann weight of 0.8822, 0.0979, 0.0111 and 0.0038. Fig. 2(a–d) show the time-evolution of the expectation values of the C–I bond distance  $R$  and the umbrella angle  $\theta$  from the four eigenstates. It can be seen that for each state the vibrational wave packet is launched from the minimum value of  $R$  and the maximum value of  $\theta$ . Thus,  $\langle R(t) \rangle$  initially evolves towards larger C–I bond distance and  $\langle \theta(t) \rangle$  evolves towards smaller C–H–I umbrella angle. The results here are in sharp contrast the experimental observations, in which the wave packet is launched from the outer turning point, i.e.  $\langle R(t=0) \rangle$  is a maximum. It should be noted that the initial state of  $\text{CH}_3\text{I}$  in the experiment is a mixed state, not a pure state as has been done in the calculation. As aforementioned, the first four states of  $\text{CH}_3\text{I}$  all have nonnegligible populations at 353 K. However, it is infeasible to determine the phase difference among the four states under the current theoretical framework.

### 4. Conclusions

In this work, three two-dimensional potential energy surfaces along the C–I bond length and the H–C–I umbrella angle, describing the

**Table 2**

Ionization energy of the ground state of  $\text{CH}_3\text{I}^+$  without spin-orbit coupling and dissociation energies of  $\text{CH}_3\text{I}^+$  with spin-orbit coupling. DE1 corresponds to the dissociation products  $\text{CH}_3^+ + \text{I}({}^2\text{P}_{3/2})$  and DE2 to the dissociation products  $\text{CH}_3 + \text{I}^+({}^3\text{P}_2)$ .  $\text{CH}_3^+$  and  $\text{CH}_3$  are both in their ground states.

	IE/eV			DE1/eV	DE2/eV
	$X^2E_{3/2}$	$A^2A_1$		$\text{CH}_3^+ + \text{I}({}^2\text{P}_{3/2})$	$\text{CH}_3 + \text{I}^+({}^3\text{P}_2)$
ADC(3) [36]	9.48	12.36	CCSD(FC)/DGP [21]	2.45	3.05
Exp. [11]	$9.540 \pm 0.004$	$11.949 \pm 0.007$	CASPT2 [26]	3.00	3.18
Exp. [37]	$9.5386 \pm 0.0006$	–	Exp. [35]	2.64	3.36
Exp. [21]	$9.543 \pm 0.005$	–	This work	2.84	3.52
Exp. [38]	$9.48 \pm 0.03$	–			
This work	9.50	12.33			

**Table 3**

Comparison of the computational and experimental energies (in  $\text{cm}^{-1}$ ) of the umbrella and C–I stretching modes of  $\text{CH}_3\text{I}$  and  $\text{CH}_3\text{I}^+$ . The theoretical energies are obtained on the corresponding two-dimensional PESs.

$\text{CH}_3\text{I}$ (ground state)	Calc.	Exp. [39]
Umbrella	1281	1252
C–I stretching	538	533
$\text{CH}_3\text{I}^+$ (ground state)	Calc.	Exp. [39]
Umbrella	1356	1257
C–I stretching	492	480
$\text{CH}_3\text{I}^+$ (first excited state)	Calc.	Exp. [39]
Umbrella	1264	1192
C–I stretching	312	294

ground electronic state of  $\text{CH}_3\text{I}$  and the ground and first excited electronic states of  $\text{CH}_3\text{I}^+$ , have been constructed using the neural network method. The ab initio energies were calculated at the level of the Davidson corrected internally contracted multireference configuration interaction (MRCI + Q) with the aug-cc-pVTZ basis set for the atoms C and H and the aug-cc-pvtz-pp basis set for the atom I. The calculated ionization energy of  $\text{CH}_3\text{I}^+$  and the dissociation energies to the dissociation products  $\text{CH}_3^+ + \text{I}({}^2\text{P}_{3/2})$  and  $\text{CH}_3 + \text{I}^+({}^3\text{P}_2)$  agree well with the available experimental results. In addition, the fundamental frequencies of the umbrella mode and the C–I stretching mode on the ground electronic state of  $\text{CH}_3\text{I}$  and the ground and first excited state of  $\text{CH}_3\text{I}^+$  are in good consistent with experimental measurements, indicating a high accuracy of the newly constructed potential energy surfaces.

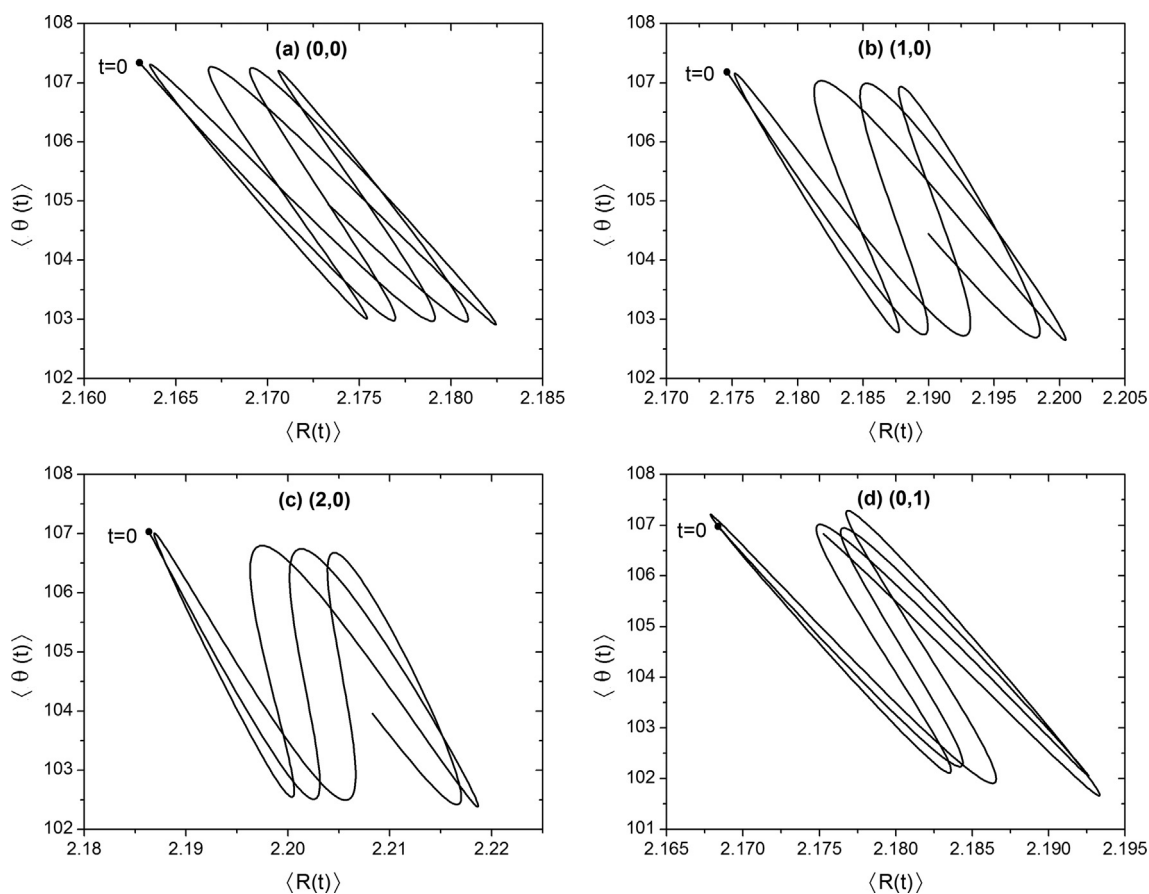


**Fig. 2.** Time-evolution of the vibrational wave packet induced by  $R$ -selective depletion along the C–I bond distance  $R$  and the umbrella angle  $\theta$ . The vibrational wave packet is generated by the strong-field ionization of the state  $(n_1, n_2)$  of  $\text{CH}_3\text{I}$ . The two quantum numbers  $n_1$  and  $n_2$  in the bracket denote excitations in the C–H stretching mode and the umbrella mode.

## Acknowledgements

This work is supported by the National Natural Science Foundation of China (Grant No. 21603266 to H. Song and 21773297 to M. Yang).

## References

- [1] Q. Shi, C. Marandino, G. Petrick, B. Quack, D. Wallace, *J. Geophys. Res. Oceans* 119 (2014) 8242.
- [2] B. Akermark, H. Johansen, B. Roos, U. Wahlgren, *J. Am. Chem. Soc.* 101 (1979) 5876.
- [3] G. McFiggans, J.M.C. Plane, B.J. Allan, L.J. Carpenter, H. Coe, C. O'Dowd, *J. Geophys. Res. [Atmos.]* 105 (2000) 14371.
- [4] C.D. O'Dowd, K. Hämeri, J. Mäkelä, M. Väkeva, P. Aalto, G. de Leeuw, G.J. Kunz, E. Becker, H.-C. Hansson, A.G. Allen, R.M. Harrison, H. Berresheim, C. Kleefeld, M. Geever, S.G. Jennings, M. Kulmala, *J. Geophys Res Atmos* 107 (2002) PAR 12.
- [5] L.J. Carpenter, W.T. Sturges, S.A. Penkett, P.S. Liss, B. Alicke, K. Hebestreit, U. Platt, *J. Geophys. Res. [Atmos.]* 104 (1999) 1679.
- [6] D. Davis, J. Crawford, S. Liu, S. McKeen, A. Bandy, D. Thornton, F. Rowland, D. Blake, *J. Geophys. Res. [Atmos.]* 101 (1996) 2135.
- [7] S. Solomon, R.R. Garcia, A.R. Ravishankara, *J. Geophys. Res. [Atmos.]* 99 (1994) 20491.
- [8] D. Xie, H. Guo, Y. Amatatsu, R. Kosloff, *J. Phys. Chem. A* 104 (2000) 1009.
- [9] D.C. McGilvery, J.D. Morrison, *J. Chem. Phys.* 67 (1977) 368.
- [10] M. Lee, M.S. Kim, *J. Chem. Phys.* 127 (2007) 124313.
- [11] L. Karlsson, R. Jadrny, L. Mattsson, F.T. Chau, K. Siegbahn, *Phys. Scr.* 16 (1977) 225.
- [12] G. Bieri, L. Asbrink, W. Vonniessen, *J. Electron Spectrosc. Relat. Phenom.* 27 (1982) 129.
- [13] S.P. Goss, D.C. McGilvery, J.D. Morrison, D.L. Smith, *J. Chem. Phys.* 75 (1981) 1820.
- [14] S.P. Goss, J.D. Morrison, D.L. Smith, *J. Chem. Phys.* 75 (1981) 757.
- [15] Y.J. Bae, M.S. Kim, *J. Chem. Phys.* 128 (2008) 124324.
- [16] J.H.D. Eland, R. Frey, A. Kuestler, H. Schulte, B. Brehm, *Int. J. Mass Spectrom. Ion Processes* 22 (1976) 155.
- [17] D.M. Mintz, T. Baer, *J. Chem. Phys.* 65 (1976) 2407.
- [18] I. Powis, *Chem. Phys.* 74 (1983) 421.
- [19] M. Grutter, J.M. Michaud, F. Merkt, *J. Chem. Phys.* 134 (2011) 054308.
- [20] W.A. Chupka, S.D. Colson, M.S. Seaver, A.M. Woodward, *Chem. Phys. Lett.* 95 (1983) 171.
- [21] R. Loch, D. Dehareng, K. Hottmann, H.W. Jochims, H. Baumgartel, B. Leyh, *J. Phys. B: At. Mol. Opt. Phys.* 43 (2010) 105101.
- [22] A. Hoxha, R. Loch, B. Leyh, D. Dehareng, K. Hottmann, H.W. Jochims, H. Baumgartel, *Chem. Phys.* 260 (2000) 237.
- [23] R. Loch, B. Leyh, K. Hottmann, H. Baumgartel, *Chem. Phys.* 220 (1997) 217.
- [24] U. Hollenstein, H. Palm, F. Merkt, *Rev. Sci. Instrum.* 71 (2000) 4023.
- [25] U. Hollenstein, R. Seiler, H. Schmutz, M. Andrist, F. Merkt, *J. Chem. Phys.* 115 (2001) 5461.
- [26] S.M. Poullain, D.V. Chicharro, J. Gonzalez-Vazquez, L. Rubio-Lago, L. Banares, *PCCP* 19 (2017) 7886.
- [27] Z. Wei, J. Li, L. Wang, S.T. See, M.H. Jhon, Y. Zhang, F. Shi, M. Yang, Z.-H. Loh, *Nat. Commun.* 8 (2017) 735.
- [28] A.B. Alekseyev, H.P. Liebermann, R.J. Buenker, D.B. Kokh, *J. Chem. Phys.* 112 (2000) 2274.
- [29] S.R. Langhoff, E.R. Davidson, *Int. J. Quantum Chem.* 8 (1974) 61.
- [30] H.-J. Werner, P.-J. Knowles, G. Knizia, F.R. Manby, M. Schuetz, *WIREs Comput. Mol. Sci.* 2 (2012) 242.
- [31] B.O. Roos, P.R. Taylor, P.E.M. Siegbahn, *Chem. Phys.* 48 (1980) 157.
- [32] L.M. Raff, M. Malshe, M. Hagan, D.I. Doughan, M.G. Rockley, R. Komanduri, *J. Chem. Phys.* 122 (2005) 84104.
- [33] M.V. Ammosov, N.B. Delone, V.P. Krainov, *Sov. Phys. JETP* 64 (1986) 1191.
- [34] Y.J. Bae, M.S. Kim, *ChemPhysChem* 9 (2008) 1709.
- [35] Y.M. Wang, S. Zhang, Z.R. Wei, B. Zhang, *J. Phys. Chem. A* 112 (2008) 3846.
- [36] D.M.P. Holland, I. Powis, G. Ohrwall, L. Karlsson, W. von Niessen, *Chem. Phys.* 326 (2006) 535.
- [37] M. Lee, Y.J. Bae, M.S. Kim, *J. Chem. Phys.* 128 (2008) 044310.
- [38] R.A.W. Johnstone, F.A. Mellon, *J. Chem. Soc. Faraday Trans. 2* (68) (1972) 1209.
- [39] NIST Computational Chemistry Comparison and Benchmark Database, NIST Standard Reference Database Number 101 Release 18, October 2016. <http://cccbdb.nist.gov/>.